Colloids and Surfaces A: Physicochemical and Engineering Aspects 652 (2022) 129822

Contents lists available at ScienceDirect

Colloids and Surfaces A: Physicochemical and Engineering Aspects

journal homepage: www.elsevier.com/locate/colsurfa

Formation of gem-like dispersions of soft crystallites in water by vesicles of a cationic surfactant

An-Hsuan Hsieh, Elias I. Franses, David S. Corti *

Davidson School of Chemical Engineering, Purdue University, West Lafayette, IN 47907-2100, USA

GRAPHICAL ABSTRACT

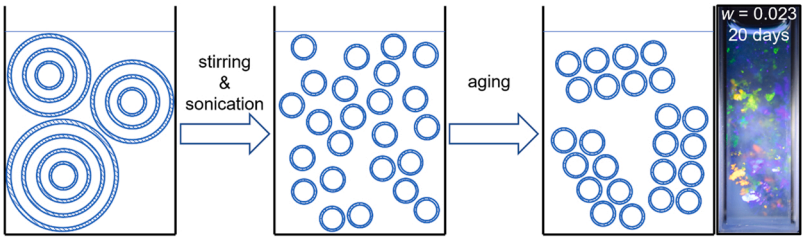

ARTICLE INFO

Keywords:
Vesicles
Sedimentation
Iridescence
Light scattering

ABSTRACT

A first discovery of iridescent liquid-like aqueous vesicle dispersions formed from the cationic surfactant didodecyldimethylammonium bromide (DDAB) is reported. Iridescence arises for some solid crystallites, thin films, and colloidal crystals, but has not yet been observed in systems that in effect remain liquid-like. Visual observations and spectroturbidimetry (ST) at wavelengths of 350–700 nm were used to determine vesicle sizes and microstructure formation in dispersions for DDAB weight fractions w between 0.020 and 0.030. The DDAB vesicle dispersions exhibited iridescent colors for w = 0.023–0.027, due to the formation of "soft" crystallites formed by self-assembled vesicles. Effective vesicle radii from 30 to 60 nm were inferred from the ST measurements. The volume fractions of the vesicles ϕ_v and their effective volume fractions ϕ_v*, which account for the electrostatic double layers around a vesicle, were also estimated. The high values of ϕ_v* for the iridescent dispersions indicate that they contain neighboring vesicles with highly overlapping electrostatic double layers, even though their values of ϕ_v remain relatively low. Hence, strong electrostatic repulsive interactions arise between the vesicles, which probably drive the formation of "soft" crystallites, and thus the observed iridescence. Nevertheless, these "soft" crystallites, which could be easily broken up but were quick to reform, remain suspended. Consequently, these vesicle dispersions still flowed as a bulk dispersion with a high viscosity; the dispersion as a whole remained liquid-like or as a "liquid gem", in contrast to what occurs to the other colloidal crystals made of rigid colloids. Beside their beautiful appearances, these DDAB vesicle dispersions also act as effective stabilizers of dense silica suspensions against sedimentation even at relatively low values of w.

* Corresponding author.
E-mail address: dscorti@purdue.edu (D.S. Corti).

https://doi.org/10.1016/j.colsurfa.2022.129822
Received 21 April 2022; Received in revised form 26 July 2022; Accepted 27 July 2022
Available online 28 July 2022

1. Introduction

We have been studying the use of aqueous dispersions of vesicles formed from the cationic surfactant didodecyldimethylammonium bromide, or DDAB, as possible stabilizers of dense particle suspensions against sedimentation [1–5]. Recently, we unexpectedly discovered that some aqueous vesicle dispersions of DDAB exhibit iridescent colors similar to those found in natural gemstones. An iridescent color is a particular type of structural color. Some authors use these terms interchangeably [6–8]. Here, we prefer the term "iridescent" because it implies diffraction more clearly. To our knowledge, this is the first example of such a phenomenon in a system that is in effect liquid-like. In contrast, most known natural materials that show beautiful iridescent colors [9,10], such as precious stones, jewels and gems, are fully crystalline solids. Iridescent colors are also exhibited by some thin solid films, or even by some feathers of birds or wings of butterflies [11–13]. Here, the iridescent colors appear when the vesicles self-assemble to form soft crystallites that nonetheless remain suspended in the aqueous medium, and are only observed across a narrow range of DDAB concentrations, or weight fractions w.

Several authors have reported formation of colloidal crystals by spherical polymer (polymethylmethacrylate (PMMA) or polystyrene (PS)) particles [14–21]. These crystallites often deposited to the bottom of the container. Their flowability was not the major focus of these studies. By contrast, the DDAB vesicle crystallites studied here are flowable in a tube and remain suspended indefinitely. Moreover, they can be easily mixed with other dense colloidal particles, which alone would sediment, to slow down or completely prevent them from sedimenting. The crystallite structures could be broken partially upon mixing or shearing but they could reform spontaneously.

Unilamellar "spherical" vesicles, or simply "vesicles", formed from various surfactants or lipids in water have been studied extensively [22–25]. These vesicles are comprised of a single closed bilayer of surfactant, with water both inside and outside. They are usually formed from double chain surfactants, such as DDAB, which is cationic, or some phospholipids, which are zwitterionic [1,26–28]. One key condition for the formation of vesicles is the ability of the surfactant to form with water lamellar liquid crystalline phases, which contain ordered multi-bilayer onion-like structures or "liposomes." (Note: some authors refer to vesicles, as we have defined them, as liposomes [23].) A second condition for vesicle formation is that the hydrocarbon interiors of the bilayers should still be fluid-like. This latter condition usually occurs above a certain temperature, known as gel-to-liquid crystalline, or chain-melting, temperature [29–32]. Above this temperature, the hydrocarbon chains are fluid-like and DDAB exhibits this behavior in water at room temperature [33–36]. Vesicles also usually do not form spontaneously from liposomes [5]. An input of mechanical energy, either in the form of stirring (method 1), or shearing through porous membranes (method 2), or ultrasonication (method 3), is needed to produce vesicles starting from a dispersion of liposomes. Although method 1 can be used to form some DDAB vesicles in water (along with liposomes), the use of method 2 or method 3 after method 1 is needed to produce DDAB vesicles exclusively, as shown recently [1,5]. In addition, the dispersion medium affects the resulting vesicle sizes. In 0.01 M NaBr solution, DDAB vesicles produced via method 2 or 3 have larger sizes than the ones produced via the same method in water [5].

DDAB vesicle dispersions generated via method 1 have been shown capable of stabilizing aqueous suspensions of solid particles, such as ~300 nm particles of high-density titania, against sedimentation [1], when the volume fraction of vesicles ϕ_v is quite high. For $w \approx 0.010$–0.020, $\phi_v \approx 0.35$–0.69 [1,2], indicating that the DDAB vesicles (estimated from cryo-TEM images to be around 500 nm in diameter) are close-packed spheres or deformed spheres as in a foam. These vesicle dispersions generate a highly non-Newtonian fluid that has a very high shear viscosity at the low shear stresses generated by the settling of solid colloidal particles. Yet, at the much higher shear stresses that typically arise for flow through a tube of macroscopic dimensions, the DDAB vesicle dispersions have a much lower shear viscosity. This strongly shear-thinning behavior makes these DDAB vesicle dispersions particularly useful in stabilizing various inks used in inkjet printing [1,3].

In this article, we present results for DDAB vesicle dispersions in water prepared with method 1 followed by method 3 for the higher weight fractions of $w = 0.020$–0.030. Iridescent colors are only observed at $w = 0.023$–0.027. The dispersions at $w < 0.023$ or $w = 0.030$ show no iridescent colors. The $w = 0.030$ dispersion is presumed to have such a high concentration of liquid crystallites after stirring that few vesicles may form after sonication; this dispersion is probably no longer water-continuous, because the pure liquid crystalline phase boundary of DDAB-water is at $w \approx 0.040$ as shown by X-ray scattering [26]. In addition, and along with their striking appearance, the DDAB dispersions at $w = 0.020$–0.030 are shown to be comparable stabilizers against sedimentation of dense colloidal particles as those dispersions prepared only by method 1 with $w < 0.020$. The unique properties of these more concentrated DDAB vesicle dispersions are due to the increased volume fraction of the vesicles (when present at $w < 0.030$) and the strong and long-range electrostatic repulsive interactions which develop between them, and arise because of the low DDAB solubility in water and the low ionic strength of the aqueous solution surrounding the vesicles.

We present below further details about the method of preparation of the DDAB vesicle dispersions in water. We also show photographs of various DDAB dispersions, viewed at different scattering angles θ, and provide spectroturbidimetry (ST) data as a function of the time t after preparation. In addition, the ST data are used to estimate the average vesicle sizes from light scattering theory, as well as yield information about the stability and reversibility of the crystalline structures that presumably appear when iridescence is observed [4,5]. Finally, we demonstrate the ability of these dispersions to slow down or prevent the sedimentation of monodisperse spherical silica particles with nominal diameters of 750 nm.

2. Methods and experimental details

2.1. Dispersion and suspension preparation methods

Ultrapure water, with resistivity of ca. 18.0 MΩ•cm, obtained from a Milli-Q water system from Millipore®, was used. DDAB in powder form, with a purity of 98 %, was purchased from Eastman Kodak. Aqueous DDAB dispersions were prepared at ca. 23 °C by first mixing DDAB with water to a total of 5 g at $w = 0.020$–0.030 and then waiting 30 min to allow hydration of the DDAB crystals to form the lamellar liquid crystallites. Afterwards, the samples were stirred at a stirring rate of 900 rpm for 2 h with a nearly cylindrical magnetic stirring bar of length 12 mm and diameter 3 mm. Then, the samples were sonicated for 15 min in a Branson 3510 sonication bath at a frequency of 40 kHz at 25 ± 2 °C. Monodisperse spherical silica particles with a diameter d_{silica} of 750 nm and a density ρ_{silica} of 2.0 g/cm^3 were obtained from Superior Silica (Tempe, AZ) as a dry powder. Aqueous silica suspensions were prepared by stirring, as above, and then followed by sonication for 2 h, to ensure that the particles were fully dispersed as single spheres.

2.2. Characterization of DDAB dispersions

For the visual observations and spectroturbidimetry measurements, 3 g aliquots of each sample were loaded into square quartz cuvettes (Hellma, 111-QS) with four transparent windows. The cuvettes had a height of 46 mm, an internal width, and thus optical path length, of 10 mm, and an external width of 12.5 mm. The samples were observed and photographed under two illumination conditions, either with diffuse overhead room light from fluorescent light bulbs or with a flashlight with a directional white light-emitting diode (LED). For the latter, the observations were made at various scattering angles from 20° to 160°. A digital camera (Nikon D5300) with a resolution of 24.4 megapixels and a

CMOS sensor was used.

Sample absorbances A were due to scattering only, since DDAB is nonabsorbing over the wavelengths $\lambda_0 = 350–700$ nm. The absorbance spectra were measured with the Agilent Cary 60 UV-Vis spectrophotometer at 23 ± 1 °C. As indicated in Fig. 1, each absorbance spectrum was determined for a small portion of the sample, which is traversed by the incident beam through a cross-sectional square area of 1 mm^2. For each sample, three spectra were obtained consecutively, with typical differences less than 0.5 %, and the average is reported here.

3. Results and discussion

3.1. Photographs of key DDAB dispersions

DDAB dispersions were visually observed and photographed for times up to 20 days after preparation (Figs. 1 and 2). The appearances of these DDAB vesicle dispersions resemble those of sterically-stabilized polymer (PMMA) nanospheres with radii 305 ± 10 nm [21]. Such particles were inferred to behave as hard spheres. For each w, three separate DDAB dispersions were prepared, and all visual observations appeared to be identical. A summary of some key observations is given below.

At 14 days after preparation, the dispersion at $w = 0.020$ looked dark with room light. With LED illumination, it showed bluish scattering colors, which varied with θ. Moreover, it looked heterogeneous, indicating some settling that formed two layers. By contrast, at $w = 0.023$,

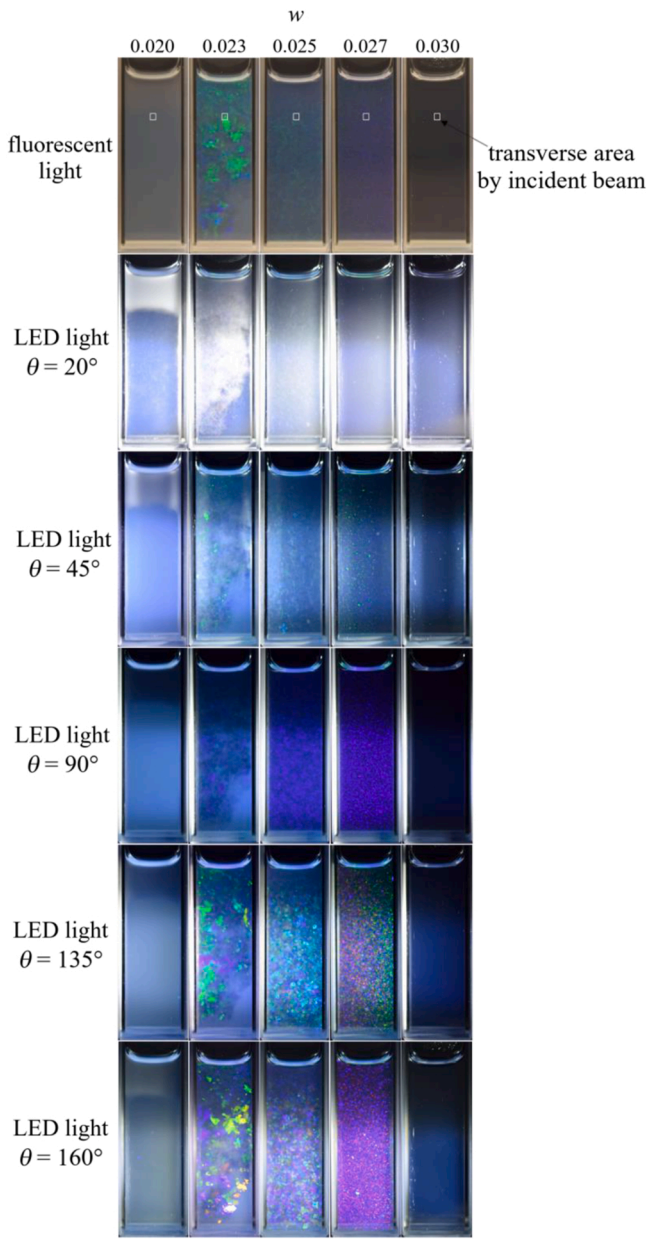

Fig. 1. Photographs of DDAB dispersions at various weight fractions w, 14 days after their preparation. The photographs were obtained with either fluorescent light or white LED light illumination at several scattering angles θ. The little squares in the top row of photographs indicate the location of the incident light beam in the ST instrument used.

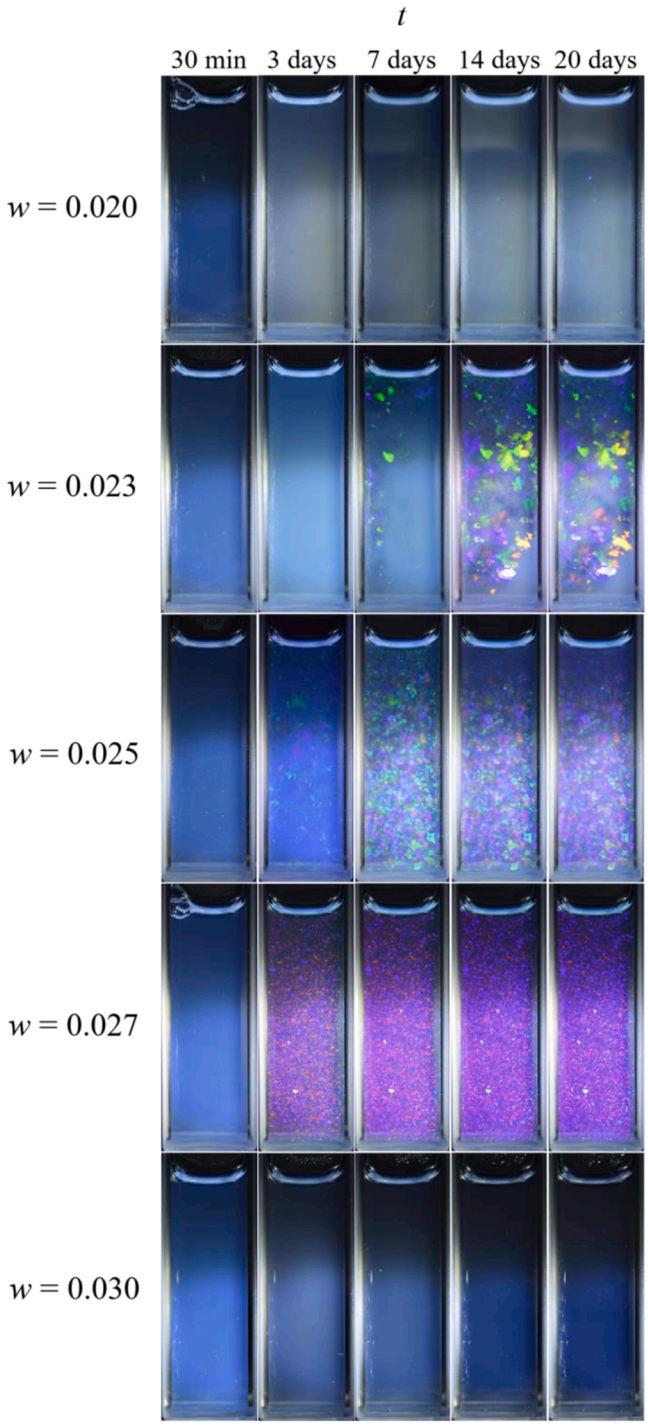

Fig. 2. Photographs of DDAB dispersions obtained at various weight fractions at various times after their preparation, with white LED light illumination at a scattering angle $\theta = 160°$; see also Fig. 1.

the dispersion showed some bluish colors and some green areas. With LED illumination, this dispersion showed inhomogeneous bluish and white colors at $\theta = 20^\circ$ and 90°, and iridescent colors at $\theta = 45^\circ$, 135°, and 160°. The dispersion at $w = 0.025$ behaved similarly to $w = 0.023$. At $w = 0.027$, the dispersion showed purplish and greenish colors at nearly all values of θ. At $w = 0.030$, no iridescent colors were seen; the sample looked transparent.

The appearances of all the dispersions varied with time (Fig. 2), indicating slow changes in vesicle sizes, or evolving vesicle-vesicle interactions, or both. The vivid iridescent colors appeared only after 3 days at $w = 0.025$ and 0.027 or after 7 days at $w = 0.023$. In Fig. 2, only the images at $\theta = 160^\circ$ are shown. Additional images at other scattering angles are presented in the Supplementary Information, SI (Figs. S1–S4).

3.2. Spectroturbidimetry results

The absorbances of the DDAB dispersions were measured at wavelengths λ_0 from 350 nm to 700 nm at various times after preparation (Figs. 3 and 4). The absorbance A is equal to $\log(e)\tau = \log(e)\tau^{**}wl$, where e is the base of the natural logarithm, τ is the turbidity, l is the optical path length and $\tau^{**} = \tau/wl$ is the specific turbidity [4,37]. The specific turbidity depends on the vesicle sizes and on the inter-vesicle structural correlations, which arise because of vesicle-vesicle interactions. When the dispersions are sufficiently dilute, such that the vesicles are both randomly distributed (i.e., there are no inter-vesicle correlations due to negligible interactions, so that the scattering of each vesicle is independent) and their scattering is single (and not multiple), τ^{**} is independent of w (while A is proportional to w) and depends only on the vesicle sizes, as shown recently [4,5]. Moreover, τ^{**} for these DDAB vesicles is well-described by the "Rayleigh-Debye-Gans" (RDG) scattering theory, since the effective relative refractive index of the vesicles $m_v = n_v/n_m$ is very close to 1 and the product of $(m_v - 1)$ times the dimensionless parameter $4\pi n_m a_v/\lambda_0$ is also much less than 1, where n_m is the refractive index of water, n_v is the effective refractive index of a vesicle and a_v is the radius of the vesicle [4,38].

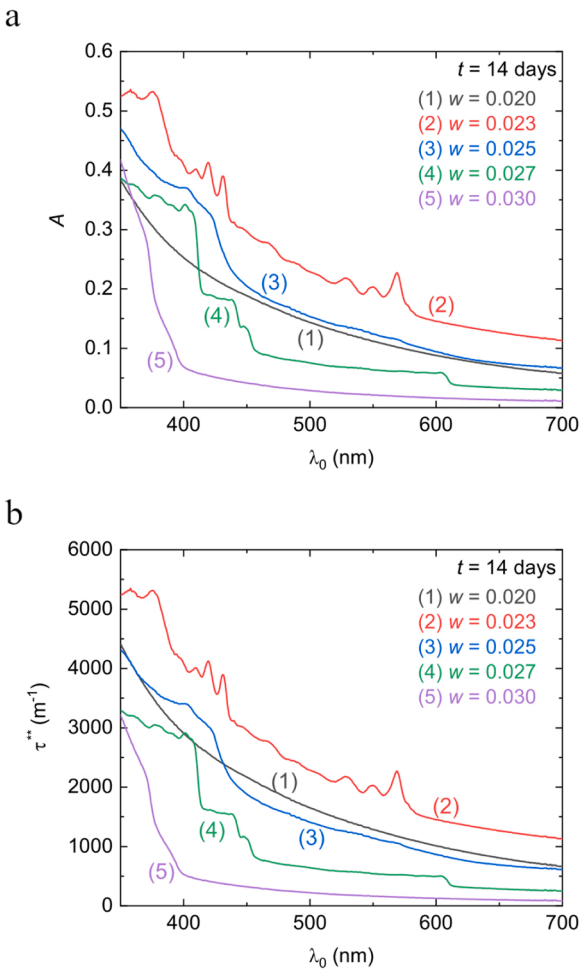

Fig. 3. (a) Absorbance spectra and (b) specific turbidity spectra of DDAB dispersions for $w = 0.020$–0.030 and 14 days after their preparation; see also Fig. 1.

The data in Fig. 3 show clearly that A was not proportional to w, or that τ^{**} varied with w. Hence, the vesicles positions were highly correlated due to strong vesicle-vesicle interactions. The $A(\lambda_0)$ curve for $w = 0.020$ was "smooth," as may be expected for an inter-vesicle structure that was non-crystalline [4]. By contrast, the $A(\lambda_0)$ curves for $w = 0.023$, 0.025, and 0.027, were quite "bumpy," suggesting that the inter-vesicle structures had become more solid-like or crystalline. This bumpiness was also highly correlated with the appearance of the iridescent colors in these samples, which arose from the local crystallinity that had developed within these colored areas. Even though the sampled areas were small, the absorbances reported here were nevertheless typical of the entire samples. By determining the absorbances at different heights, the samples were found to be only slightly heterogeneous.

The bumpy spectral curves were not observed at 30 min after preparation, but appeared after 3–7 days for $w = 0.023$ and 0.025, and less than 3 days for $w = 0.027$. Thus, the crystalline vesicle dispersion microstructures giving rise to iridescence took some time to form. These spectral shapes, and their corresponding colors, were indicative of a unique feature of these iridescent vesicle crystallites, which visually resembled the colors observed in some solid gems. Furthermore, A generally increased with time, and reached nearly constant values after about 14–20 days for $w = 0.020$, 0.027, and 0.030, suggesting that the dispersion microstructures were still changing over this time. Moreover, the particular shapes of the bumpy spectra for $w = 0.023$, 0.025, and 0.027 remained essentially unchanged after first appearing, even though the absorbances continued to change (for several more days). Hence, the vesicle crystalline microstructure, once formed, apparently remained the same, although the overall sizes of these crystallites were still evolving.

The spectral curves for $w = 0.030$ were quite different than for the other samples. For this concentration, no bumps or iridescent colors were seen, and A first increased with time and then decreased with time. The spectral curves were smooth at larger wavelengths and showed a very fast decrease with λ_0 from 350 to 400 nm. Hence, at $w = 0.030$, the dispersion microstructure was quite different compared to those at $w = 0.023$–0.027.

To further understand the physical interactions and microstructures of these dispersions, the vesicle sizes must be known. To do so reliably with ST, only for dilute enough dispersions may one safely infer vesicle sizes using the current version of the RDG light scattering theory for vesicles [4,5]. The theory is based on the single and independent, or uncorrelated, scattering of the particles. For single and independent scattering, τ^{**} is independent of w, and the current RDG relations for vesicles with a given value a_v can be reliably compared to ST data to obtain that vesicle radius which yields the best fit, or the effective average vesicle radius (see the SI for further details). For this reason, each dispersion was diluted to lower w-values, until τ^{**} was found to be independent of w, reached for $w \leq 0.0010$. The effective average vesicle radii were determined for each dispersion both 10 and 30 days after preparation. The results are given in Table 1 (with further details of how they were obtained from the RDG theory provided in the SI). The average vesicle radii ranged from 30 to 40 nm after 10 days, and from 37 to 62 nm after 30 days, indicating only a slow size increase with time. The small size increase is most likely not due to vesicle coagulation and coalescence, which are prevented by the electrostatic repulsions, but probably because of Ostwald ripening, with mass transfer occurring

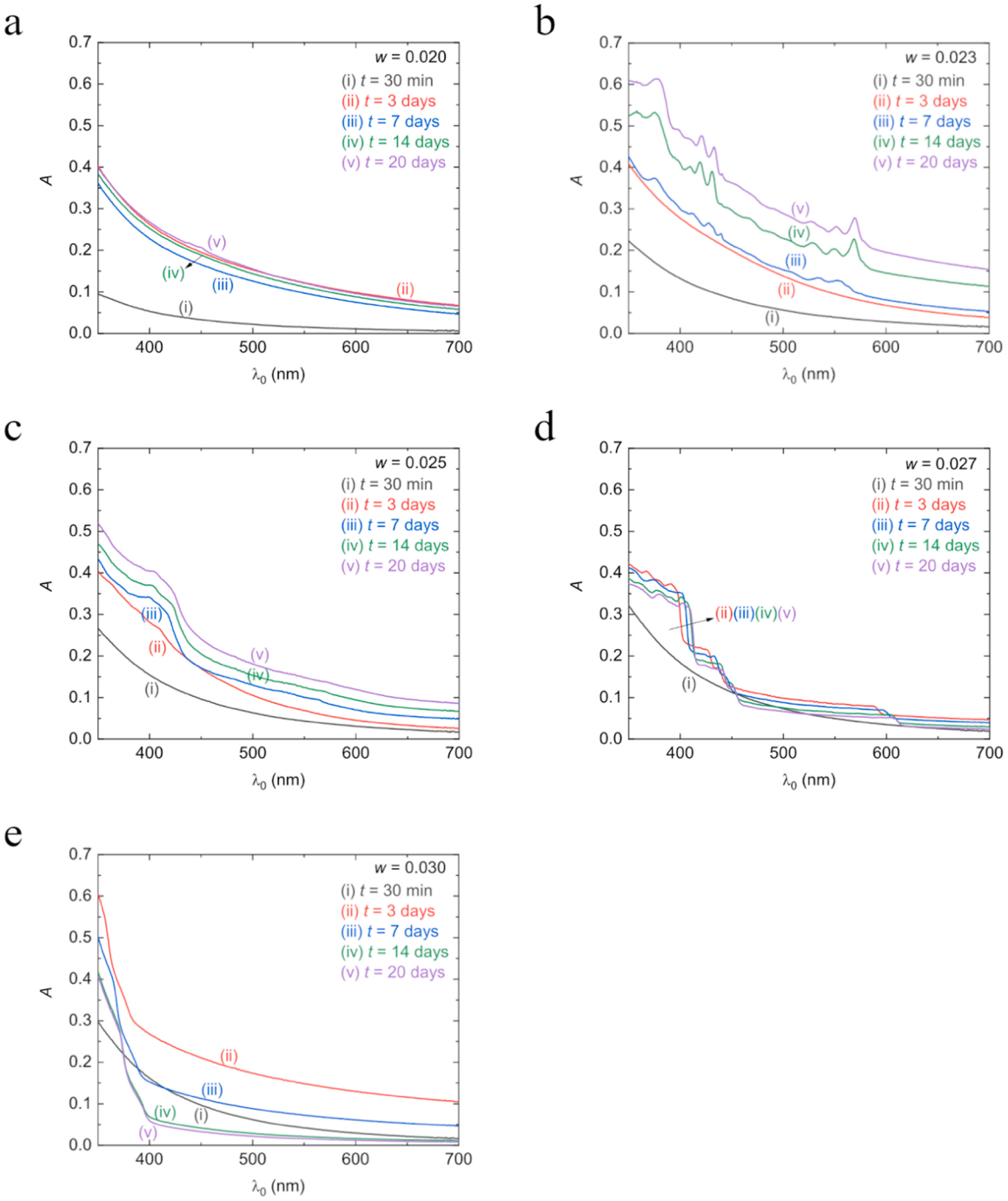

Fig. 4. Absorbance spectra of DDAB dispersions at various times after their preparation for w = (a) 0.020, (b) 0.023, (c) 0.025, (d) 0.027, and (e) 0.030. Some photographs of these dispersions are also shown in Fig. 2.

Table 1
Average effective vesicle radii a_v of DDAB dispersions at w = 0.020–0.030, and at 10 and 30 days after their preparation.

	a_v (nm)	
w	10 days	30 days
0.020	40	62
0.023	30	37
0.025	35	51
0.027	34	43
0.030	40	50

from smaller to larger vesicles. This change in size affects slightly the number of vesicles, the microstructures of the crystallites, and the resulting colors. Nevertheless, the observed changes in A with time were primarily due to some growth of the crystallites, and not to significant changes in the primary vesicle sizes.

Finally, several tests were done to examine the stability of the crystalline microstructures to mixing and shearing, and the reversibility of their formation. The dispersions at w = 0.023–0.027 were mixed gently, by turning them upside-down 10 times in succession. The iridescent colors disappeared, and the absorbance spectra became non-bumpy after this mixing disturbance (see SI, Figs. S5 and S6). Yet after one day, colors and bumpy spectra started to reappear. These results indicate

that the crystalline microstructures initially broke down, but then started reforming. Nevertheless, somewhat different colors were seen, and the visual observations of these samples suggest that the reformed vesicle crystallites had smaller sizes than before the mixing disturbance. For example, at $w = 0.025$, the iridescent colors changed from greenish to purplish due to the size decrease of the microcrystallites after the structures broke down partially by the mixing. The observed changes in A after mixing indicate that the size of the microcrystallites continued to change with time (Fig. S6 in SI).

3.3. Effect of DDAB dispersions on the sedimentation of silica particles

Suspended silica particles in water or suspension droplets in water sediment depending on their particle or droplet diameter d, the density difference $\Delta\rho$ between the particles/droplets and the dispersing medium and the viscosity of the dispersing medium η. The sedimentation or terminal velocity v_{sed} of noninteracting particles can be determined from the balancing of Stokes' drag force and the buoyant and gravitational forces on an individual particle, which results in [37]

$$v_{sed} = \frac{d^2 \Delta\rho g}{18\eta} \quad (1)$$

For the spherical silica particles used in this study, with $d = 750$ nm, $\Delta\rho = 1.0$ g/cm^3 and a viscosity of water $\eta = 1.0$ cP ($g = 9.8$ m/s^2), $v_{sed} = 3.1 \times 10^{-5}$ cm/s. Hence, the sedimentation time in water for a height $h = 3.5$ cm is 31 h. If η were instead 10^5 to 10^9 cP, the sedimentation times would be 350–3.5 $\times 10^6$ years. In addition, the shear stress $\tau \approx \frac{2}{3} d\Delta\rho g$ exerted by a single silica particle was about 4.9×10^{-3} Pa (Ref. [2]). In contrast, for spherical droplets with $d = 2$ mm and $\Delta\rho = 0.02$ g/cm^3 (based on a 2.0 wt % silica suspension), $v_{sed} = 4.4$ cm/s in water. The corresponding sedimentation time for $h = 3.5$ cm is therefore 0.8 s. If η were instead 10^5 to 10^9 cP, the sedimentation times would be 22 h to 25 years.

Several experiments for testing the effect of the DDAB dispersions on the sedimentation rate of silica particles were done not by suspending the particles in DDAB dispersions, as in Ref. [1], but by the following procedure, which was chosen to avoid breaking up the vesicle crystallites. A 0.5 ml suspension of 2.0 wt % (1.0 vol%) 750 nm silica particles was placed dropwise on top of the DDAB dispersion by using a syringe. When such a silica suspension was placed on top of water, as a "control" experiment, the silica suspension as a whole settled substantially in less than 1 h (see Fig. 5). Nevertheless, some narrow rivulets of the silica suspension were observed to sediment with a velocity of about 9.4 cm/s, estimated from a video of the process (see SI for a summary of the content of the videos). By using Eq. (1), with $\eta = 1.0$ cP and $\Delta\rho = 0.02$ g/cm^3 (as portions of the suspension were sedimenting, and not the individual silica particles), the effective diameter of a sedimenting droplet of the silica suspension, $d_{droplet}$, was therefore estimated to be about 0.29 cm. Such a droplet is expected to settle to the bottom of the 3.5 cm sample height in 0.4 s.

Similar behavior, but with slower settling velocities, was observed for the $w = 0.020$ and 0.023 dispersions. From the videos of the experiments (see SI), the sedimentation velocities of the initial rivulets were estimated to be 0.77 and 0.035 cm/s, respectively. Using the same suspension droplet diameter of 0.29 cm, the corresponding estimated viscosities of the vesicle dispersions, obtained by using Eq. (1) again, were 12 and 260 cP. Furthermore, the shear stresses experienced by these falling droplets were about 0.38 Pa.

For $w = 0.025$, no rivulets were seen as the silica suspension was placed on top of the DDAB vesicle dispersion. Initially, the iridescent DDAB layer started shrinking while the silica suspension as a whole settled slightly, and remained on the top for at least 8 h. Hence, the viscosity of the vesicle dispersion was very high. Later, the top suspension layer became clearer and bluish, as the silica particles settled only inside it and as some of the DDAB vesicle dispersion was transported into this layer. During this time, the silica particles did not appear to enter the iridescent DDAB dispersion. Thus, at the low shear stresses experienced by the silica particles the viscosity of the DDAB vesicle dispersion was effectively infinite. At 23 h, and as more vesicles entered the top layer, the DDAB dispersion became diluted enough such that its viscosity began to decrease. Consequently, the vesicle dispersion could no longer support the top suspension layer, which was then observed to settle as a whole similar to $w = 0.023$ at shorter times. For $w = 0.027$, the silica layer settled similarly but more slowly as at $w = 0.025$.

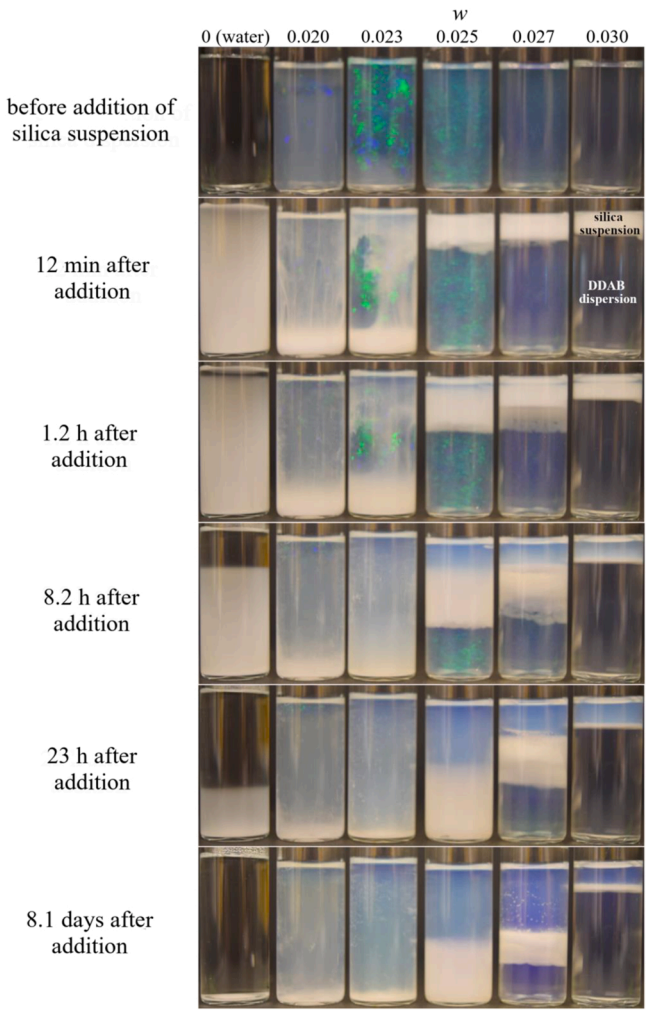

Fig. 5. Photographs of DDAB dispersions at $w = 0.020$–0.030, and 14 days after their preparation, and after 0.5 ml of a 2.0 wt % silica suspension was placed on top of each; for reference, results for water ($w = 0$) are also shown.

For $w = 0.030$, the silica suspension layer remained on top for over 8 days, and some silica particles settled inside this layer, without entering the DDAB dispersion. The thickness of this top layer increased slightly as some DDAB vesicles and water apparently diffused into it. This dispersion prevented the sedimentation of the silica particles and the suspension layer, indicating that its viscosity was effectively infinite at both the low and high shear stresses exerted by a silica particle and a suspension droplet.

3.4. Analysis of the electrostatic interactions among the vesicles and their effect on the dispersion microstructure

At the conditions of the reported experiments, each DDAB vesicle in water is surrounded by a small concentration of dissolved $DDAB^+$ and Br^- ions. Since the solubility of DDAB is about $c = 10^{-5}$ M (0.0005 wt %) [39], each ion concentration is also about 10^{-5} M, and so the ionic

strength $I \sim 10^{-5}$ N. Here, we ignore the ionic strength of 10^{-7} M of pure water at pH = 7.0, or of typical water in a laboratory with pH = 5–6. Then, with this ionic strength, the Debye length λ_D is estimated to be about 96 nm [37], which is larger than the vesicle radii (Table 1). The electrostatic potential around such a vesicle decays exponentially to zero at a distance of about $2.5\lambda_D = 240$ nm [37]. Therefore, when the average separation distance between the bilayers in two different vesicles, d_{vv}, is smaller than $2.5\lambda_D$, the vesicles-vesicle electrostatic interactions are expected to be significant. On the other hand, for $d_{vv} \geq 2.5\lambda_D$, the DDAB vesicle dispersion is effectively "dilute," as shown schematically in Fig. 6, and should behave as an uncorrelated "ideal gas." Now, the volume fraction of the vesicles ϕ_v is given by

$$\phi_v = \frac{w a_v^3}{a_v^3 - (a_v - d_b)^3}\left(\frac{\rho_{disp}}{\rho_{surf}}\right) \approx \frac{w a_v}{3 d_b} \quad (2)$$

where d_b is the bilayer thickness of a DDAB vesicle, which is 2.4 nm [26, 36], ρ_{disp} is the density of the dispersion, ca. 1.00 g/cm^3, and ρ_{surf} is the density of the DDAB surfactant bilayer, ca. 1.00 g/cm^3. We also define an effective volume fraction ϕ_v^* based on the effective maximum "interaction" radius of $a_v + 2.5\lambda_D$, which is given by

$$\phi_v^* = \frac{w(a_v + 2.5\lambda_D)^3}{(a_v + 2.5\lambda_D)^3 - (a_v + 2.5\lambda_D - d_b)^3}\left(\frac{\rho_{disp}}{\rho_{surf}}\right) \approx \frac{w(a_v + 2.5\lambda_D)}{3 d_b} \quad (3)$$

The choice of $2.5\lambda_D$, the distance beyond which electrostatic interactions are nearly negligible, leads to an upper bound (and perhaps an overestimation) of the effective volume fraction of the vesicles. Other definitions of the effective volume fraction can be employed [40–42], although Eq. (3) is straightforward to use and leads to similar qualitative insights.

Using the estimated radii provided in Table 1, for $w \leq 0.0010$, we find, as expected, that the volume fractions are quite low for these dilute dispersions, with $\phi_v \leq 0.0090$ for $a_v = 62$ nm ($w = 0.020$, 30 days) and $\phi_v^* \leq 0.042$ for $a_v = 62$ nm ($w = 0.020$, 30 days). As w, ϕ_v, and ϕ_v^* increase beyond these limits, the electrical double layers around the vesicles start to overlap (Fig. 6b), and the inter-vesicle electrostatic interactions become important. This affects the light scattering properties of the dispersions (as structural correlations arise between the vesicles), as well as their viscosities. As w increases beyond its dilute limit, the DDAB vesicle dispersions eventually become quite viscous, because the volume fraction of the vesicles increases, and in particular the effective volume fraction becomes quite high. The vesicle dispersion remained amorphous or liquid-like up to about $w = 0.020$, at which, for the measured vesicle sizes, ϕ_v ranged from 0.012 to 0.18, and ϕ_v^* ranged from 0.78 to 0.85 (Fig. 6b). At $w = 0.023$, 0.025, and 0.027, ϕ_v ranged from 0.010 to 0.13, from 0.13 to 0.19, and from 0.14 to 0.17, respectively; ϕ_v^* ranged from 0.87 to 0.89, from 0.96 to 1.0, and from 1.0 to 1.1, respectively. (With our choice of the upper bound of $2.5\lambda_D$ in Eq. (3), values of ϕ_v^* greater than the close-packed hard sphere limit of around 0.74 simply indicate that there is a significant overlap of the electrostatic double layers of the vesicles. If $2.5\lambda_D$ were replaced with λ_D in Eq. (3), a smaller estimate of the distance over which electrostatic repulsive interactions are important, the effective volume fractions of these more concentrated dispersions would instead range from 0.38 to

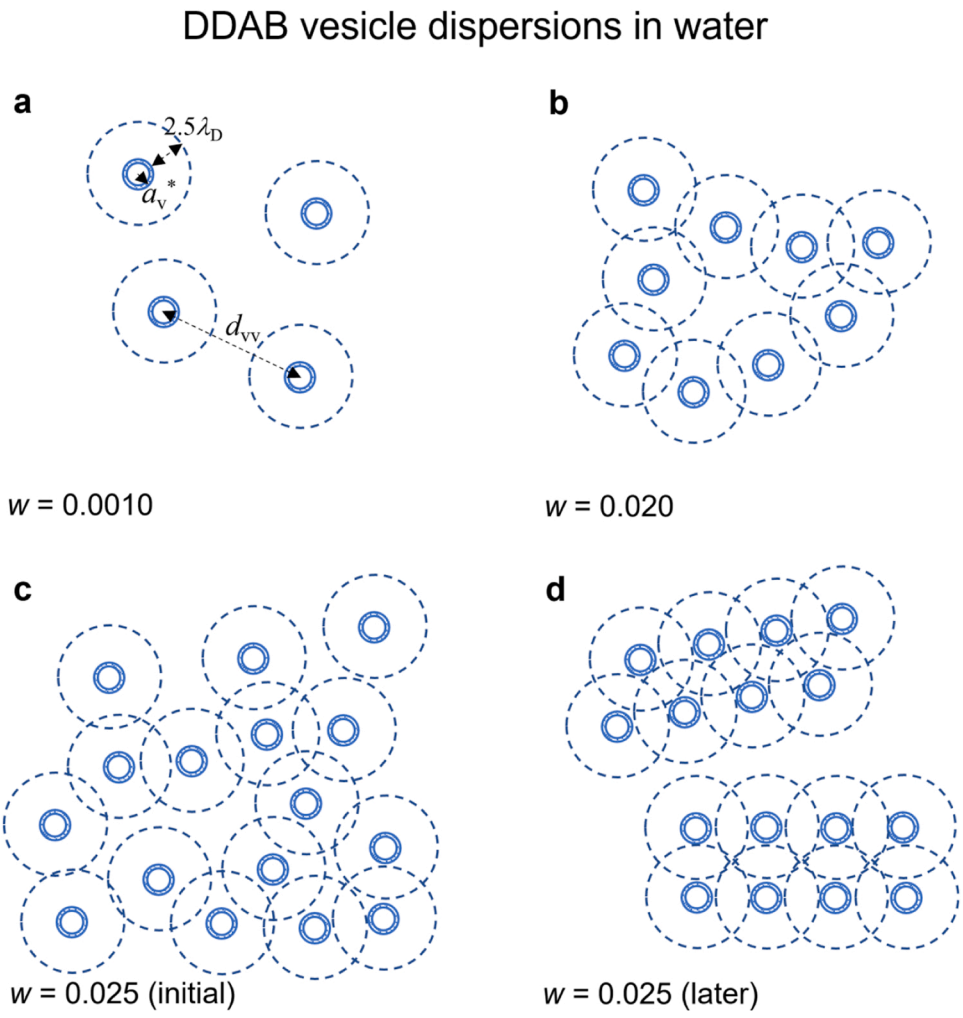

Fig. 6. Schematic diagrams of (**a**) a dilute dispersion of noninteracting DDAB vesicles in water at $w \leq 0.0010$; (**b**) of a concentrated DDAB vesicle dispersion with $w = 0.020$, with strong interacting vesicles with overlapping electric double layers and an overall amorphous structure; (**c**) of initially prepared DDAB dispersions with $w = 0.025$, with stronger vesicle-vesicle interactions (see also Fig. 1); (**d**) of DDAB dispersions with $w = 0.025$ 3 days after preparation, which form crystalline structures (see also Fig. 1).

0.61. For reference, the hard sphere fluid-solid transition is found to occur at a volume fraction of around 0.49 [43–45]).

So, while the actual volume fractions remained low, strong electrostatic interactions nonetheless arose between neighboring vesicles at these higher weight fractions. The vesicles along with their electric double layers became close-packed and therefore formed iridescent polycrystalline domains, although their inter-vesicle distances were still quite large. (This is shown schematically in Fig. 6c and d, for example, for $a_v = 35$ nm, or for $w = 0.025$ at 10 days after preparation; see SI.) Hence, these vesicles formed relatively "loose" or "soft" crystallites, which could be easily broken up, but then quickly started to reform. Moreover, these "soft" crystallites remained suspended in the aqueous medium. Consequently, these vesicle dispersions still flowed as a bulk dispersion with a high viscosity, i.e., the dispersion as a whole still remained liquid-like or as a "liquid gem". The self-assembly mechanism of these soft crystallites involves first a sequential agglomeration of the vesicles, followed by an ordering into crystallites, which remain easily broken up because the strong inter-vesicle electrostatic repulsions prevent the vesicles from touching each other. The crystalline structures cause diffraction of white light, which gives rise to the iridescent colors. Moreover, the combined effect of the dense packing of the soft crystallites and the strong electrostatic repulsions gives rise to a mechanical property of the dispersion analogous to a yield stress, which prevents many types of dense suspended particles from sedimenting. The discovery of DDAB crystallites opens up a potential research area of the determination of the resulting crystalline structures, which could be investigated by SAXS or SANS. Such studies are, however, beyond the scope of this article.

4. Conclusions

The formation of iridescent vesicle crystallites formed by close-packed DDAB vesicle dispersions in a liquid-like system has been reported. These vesicle crystallites remain suspended indefinitely and remain flowable, unlike many other colloidal crystal dispersions formed by rigid polymer colloidal particles [16,20,21]. Because of such properties, these soft vesicle crystallites can be easily mixed with dense, easy to sediment, colloidal particles which can sediment very slowly or be prevented from sedimenting completely. The visual appearances of the iridescent crystallites and the dispersions were found to vary with DDAB concentration, the times after their preparation, the illumination methods, and the viewing angles used for their observations. The absorbances due to scattering of DDAB vesicle dispersions were measured at 350–700 nm at various weight fractions w and times after their preparation. The calculated specific turbidities varied with w, indicating "dependent" scattering caused by strong physical interactions among the vesicles. Such interactions give rise to the formation of liquid-like and solid-like microstructures. By sufficiently diluting the vesicle dispersions in order to eliminate such interactions, thereby achieving single and "independent" scattering, the average effective vesicle radii were estimated from the turbidity data (following the method developed previously [4,5]). The resulting estimates for the effective volume fractions of the vesicles, which account for the electrostatic double layers surrounding a vesicle, were very high, leading to the formation of iridescent vesicle crystallites. The actual volume fractions of the vesicles (without the electrostatic double layers) were, 0.096–0.21, lower than the close-packed limit of spheres of 0.74. When assembled, the vesicle crystallites were therefore "soft"; they remained suspended in the aqueous medium, were easily broken up, and they were able to reform. Finally, the DDAB dispersions at $w \geq 0.025$ were found to substantially slow down, or completely prevent, the sedimentation of silica particles or of layers containing suspended silica particles.

CRediT authorship contribution statement

A.-H. Hsieh: Conceptualization, performed the experiments and analysis, writing. **E.I. Franses:** Conceptualization, Supervision, writing. **D.S. Corti:** Conceptualization, Supervision, writing.

CRediT authorship contribution statement

E.I.F. and D.S.C. led the research. A.-H.H. conducted the experiments and performed the analyses of the ST data. All authors participated in the discussion of the results and contributed to the writing of the manuscript.

Declaration of Competing Interest

The authors declare that they have no known competing financial interests or personal relationships that could have appeared to influence the work reported in this paper.

Data Availability

Data will be made available on request.

Acknowledgements

This work was supported by the National Science Foundation (Grant #1706305). The authors thank Professor Bryan Boudouris from Purdue University for the use of the spectrophotometer, Chung-Shuo Lee for the use of the Nikon D5300 digital camera, and Ting-Wei Liu for help with the filming of the videos.

Appendix A. Supporting information

Supplementary data associated with this article can be found in the online version at doi:10.1016/j.colsurfa.2022.129822.

References

[1] Y.J. Yang, D.S. Corti, E.I. Franses, Use of close-packed vesicular dispersions to stabilize colloidal particle dispersions against sedimentation, Langmuir 31 (2015) 8802–8808.
[2] Y.J. Yang, E.I. Franses, D.S. Corti, Effects of light dispersed particles on the stability of dense suspended particles against sedimentation, J. Phys. Chem. B 123 (2019) 922–935.
[3] E.I..Franses, D.S..Corti, Y.J..Yang, H.T..Zhao, Y..Zhao, H.S..Tom, Aqueous Ink Composition, US 10,696,044 B2. June 30, 2020, n.d.
[4] A.H. Hsieh, D.S. Corti, E.I. Franses, Rayleigh and Rayleigh-Debye-Gans light scattering intensities and spetroturbidimetry of dispersions of unilamellar vesicles and multilamellar liposomes, J. Colloid Interface Sci. 578 (2020) 471–483.
[5] A.H. Hsieh, E.I. Franses, D.S. Corti, Effects of the method of preparation and dispersion media on the optical properties and particle sizes of aqueous dispersions of a double-chain cationic surfactant, Langmuir 37 (2021) 8290–8304.
[6] S. Kinoshita, S. Yoshioka, Structural colors in nature: the role of regularity and irregularity in the structure, ChemPhysChem 6 (2005) 1442–1459.
[7] S.N. Fernandes, Y. Geng, S. Vignolini, B.J. Glover, A.C. Trindade, J.P. Canejo, P. L. Almeida, P. Brogueira, M.H. Godinho, Structural color and iridescence in transparent sheared cellulosic films, Macromol. Chem. Phys. 214 (2013) 25–32.
[8] A. Kawamura, M. Kohri, G. Morimoto, Y. Nannichi, T. Taniguchi, K. Kishikawa, Full-color biomimetic photonic materials with iridescent and non-iridescent structural colors, Sci. Rep. 6 (2016) 1–10.
[9] J.V. Sanders, Diffraction of light by opals, Acta Crystallogr. Sect. A 24 (1968) 427–434.
[10] L. Shang, Z. Gu, Y. Zhao, Structural color materials in evolution, Mater. Today 19 (2016) 420–421.
[11] C.H. Greenewalt, W. Brandt, D.D. Friel, Iridescent colors of hummingbird feathers, J. Opt. Soc. Am. 50 (1960) 1005.
[12] H. Ghiradella, Light and color on the wing: structural colors in butterflies and moths, Appl. Opt. 30 (1991) 3492.
[13] P. Vukusic, J.R. Sambles, Photonic structures in biology, Nature 424 (2003) 852–855.
[14] L.B. Chen, M.K. Chow, B.J. Ackerson, C.F. Zukoski, Rheological and microstructural transitions in colloidal crystals, Langmuir 10 (1994) 2817–2829.
[15] L. BinChen, C.F. Zukoski IV, Flow of ordered latex suspensions: Yielding and catastrophic shear thinning, J. Chem. Soc. Faraday Trans. 86 (1990) 2629–2639.
[16] A.P. Gast, Y. Monovoukas, A new growth instability in colloidal crystallization, Nature 351 (1991) 553–555.
[17] Y. Monovoukas, A.P. Gast, A study of colloidal crystal morphology and orientation via polarizing microscopy, Langmuir 7 (1991) 460–468.

[18] Y. Monovoukas, G.G. Fuller, A.P. Gast, Optical anisotropy in colloidal crystals, J. Chem. Phys. 93 (1990) 8294–8299.
[19] P.A. Rundquist, S. Jagannathan, R. Kesavamoorthy, C. Brnardic, S. Xu, S.A. Asher, Photothermal compression of colloidal crystals, J. Chem. Phys. 94 (1991) 711–717.
[20] J.H. Holtz, S.A. Asher, Polymerized colloidal crystal hydrogel films as intelligent chemical sensing materials, Nature 389 (1997) 829–832.
[21] P.N. Pusey, W. vanMegen, Phase behaviour of concentrated suspensions of nearly colloidal spheres, Nature (1986) 2–4.
[22] A.D. Bangham, R.W. Horne, Negative staining of phospholipids and their structural modification by surface-active agents as observed in the electron microscope, J. Mol. Biol. 8 (1964) 660–668.
[23] S. Šegota, D. Težak, Spontaneous formation of vesicles, Adv. Colloid Interface 121 (2006) 51–75.
[24] J.O. Eloy, M. Claro de Souza, R. Petrilli, J.P.A. Barcellos, R.J. Lee, J.M. Marchetti, Liposomes as carriers of hydrophilic small molecule drugs: Strategies to enhance encapsulation and delivery, Colloid Surf. B 123 (2014) 345–363.
[25] D.M. Patel, R.H. Jani, C.N. Patel, Ufasomes: a vesicular drug delivery, Syst. Rev. Pharm. 2 (2011) 72–78.
[26] T. Zemb, D. Gazeau, M. Dubois, T. Gulik-Krzywicki, Critical behaviour of lyotropic liquid crystals, Europhys. Lett. 21 (1993) 759–766.
[27] H.I. Petrache, S. Tristram-Nagle, D. Harries, N. Kučerka, J.F. Nagle, V.A. Parsegian, Swelling of phospholipids by monovalent salt, J. Lipid Res. 47 (2006) 302–309.
[28] J.A. Staton, S.R. Dungan, Mechanism of time-dependent adsorption for dilauroyl phosphatidylcholine onto a clean air-water interface from a dispersion of vesicles, Langmuir 34 (2018) 9961–9973.
[29] J.M. Seddon, G. Cevc, D. Marsh, Calorimetric studies of the gel-fluid (L beta-L alpha) and lamellar-inverted hexagonal (L alpha-HII) phase transitions in dialkyl- and diacylphosphatidylethanolamines, Biochemistry 22 (1983) 1280–1289.
[30] P. Saveyn, P. Van DerMeeren, M. Zackrisson, T. Narayanan, U. Olsson, Subgel transition in diluted vesicular DODAB dispersions, Soft Matter 5 (2009) 1735–1742.
[31] E. Feitosa, R.D. Adati, P. Hansson, M. Malmsten, Thermal and structural behavior of dioctadecyldimethylammonium bromide dispersions studied by differential scanning calorimetry and X-Ray scattering, PLoS One 7 (2012) 1–9.
[32] G. Bozzuto, A. Molinari, Liposomes as nanomedical devices, Int. J. Nanomed. 10 (2015) 975–999.
[33] O. Regev, A. Khan, Vesicle — lamellar transition events in DDAB-water solution, Trends Colloid Interface Sci. VIII (2007) 298–301.
[34] E. Feitosa, R.D. Adati, F.R. Alves, Thermal and phase behavior of didodecyldimethylammonium bromide aqueous dispersions, Colloids Surf. A Physicochem. Eng. Asp. 480 (2015) 253–259.
[35] E. Feitosa, Kinetic asymmetry in the gel-liquid crystalline state transitions of DDAB vesicles studied by differential scanning calorimetry, J. Colloid Interface Sci. 344 (2010) 70–74.
[36] G.A. Ferreira, W. Loh, Structural parameters of lamellar phases formed by the self-assembly of dialkyldimethylammonium bromides in aqueous solution, J. Braz. Chem. Soc. 27 (2016) 392–401.
[37] P.C. Hiemenz. Principles of Colloid and Surface Chemistry, 3rd ed., CRC Press, Boca Raton, 1997.
[38] M. Kerker, The Scattering of Light and Other Electromagnetic Radiation, Academic Press, New York, 1969.
[39] J.F.A. Soltero, F. Bautista, E. Pecina, J.E. Puig, O. Manero, Z. Proverbio, P. C. Schulz, Rheological behavior in the didodecyldimethylammonium bromide/water system, Colloid Polym. Sci. 278 (2000) 37–47.
[40] W.G. Hoover, F.H. Ree, Melting transition and communal entropy for hard spheres, J. Chem. Phys. 49 (1968) 3609–3617.
[41] L.V. Woodcock, Glass transition in the hard-sphere model and Kauzmann'S Paradox, Ann. N. Y. Acad. Sci. 371 (1981) 274–298.
[42] P. Pawel, Colloidal crystals, Contemp. Phys. 24 (1983) 25–73.
[43] B.J. Alder, T.E. Wainwright, Phase transition for a hard sphere system, J. Chem. Phys. 27 (1957) 1208–1209.
[44] L.A. Fernández, V. Martín-Mayor, B. Seoane, P. Verrocchio, Equilibrium fluid-solid coexistence of hard spheres, Phys. Rev. Lett. 108 (2012) 1–5.
[45] A. Santos, S.B. Yuste, M. López De Haro, Structural and thermodynamic properties of hard-sphere fluids, J. Chem. Phys. 153 (2020).